

Numerical Study of the Controlled Droplet Breakup by Electric Fields inside a Microfluidic Flow-focusing Device

Y. Li¹, M. Jain¹, C. Kumar², and K. Nandakumar^{1*}

¹ Cain Department of Chemical Engineering, Louisiana State University

² Center for Advanced Microstructures and Devices (CAMD), Louisiana State University

*Corresponding author: 210 ChE Building, LSU, Baton Rouge, LA, 70803, nandakumar@lsu.edu

Abstract: Droplet-based microfluidics has received extensive research interests due to its superior control over the fluid flow. Conventional passive microfluidic flow-focusing devices confront difficulties in controlling droplet sizes in dripping regime especially when the dispersed phase has a large viscosity. External electric fields have been reported as an effective tool to manipulate droplet breakup. In present study, a computational fluidic dynamics based level-set method coupled with perfect dielectric model is used to investigate the formation of viscous silicone droplets inside water. The numerical simulations have shown that the breakup process exhibits different behaviors when electric fields of various strengths are applied due to the interaction of hydrodynamics and electrodynamics.

Keywords:

Droplet-based microfluidics, microfluidic flow focusing, CFD, electric field, perfect dielectric model

1. Introduction

Droplet-based microfluidics has attracted extensive research interests due to its superior control on fluid flows¹. By introducing another immiscible fluid as the continuous phase, the operating fluid is segmented into droplets or bubbles in micro-liters sizes². Compared to the traditional single phase flows, droplet-based microfluidics provides several unique advantages such as fast mixing, reduced dispersion and no surface fouling³. These advantages have ensured droplet-based microfluidics numerous applications on DNA analysis, protein crystallization, chemical synthesis and other fields². For most of these applications, controlling droplet size and distributions is necessary. Most of the droplet-generating methods in literature are based on passive droplet breakup which utilizes geometries of the microfluidic device and fluid flows. The droplet formation process relies on the interactions

between inertial force, viscous force and surface tension force between the two phases, producing droplets comparable to device dimensions. For example, the diameter of the droplets produced in microfluidic flow-focusing devices (MFFD) approximate to the orifice size in the dripping regime⁴. If small droplets are needed, the MFFD are usually operated at high flow ratios to enhance the effect of viscous force and inertial force. However, this approach is not effective when the dispersed phase is more viscous than the continuous phase. If silicone oil with viscosity of 50 cp is used as the continuous phase while aqueous solution of 1 cp is used as the continuous phase, Nie et al. observed that the droplet sizes are marginally affected by controlling flow ratios in dripping regime⁵. For such circumstances, employing external forces are more effective in terms of controlling droplet breakup.

Recently, Link et al. has presented a robust platform of manipulating droplet-based microfluidics by introducing an external electric field⁶. They have developed modules that are able to provide fine control over individual droplets such as breakup, coalescence, sorting, etc. Such systems consist of conventional microfluidic devices and electrodes connected to high voltage direct current (DC) power supplies. Due to the different electrical such as permittivity and conductivity properties between the two phases, the electric field induces surface charges including polarization and free charges on the interface. The interaction of the electric field and surface charges results in electric forces (its stress is named as Maxwell stress) on the interface, which provides an additional mean to control droplet breakup. If the electric field is configured properly, the resulted Maxwell stress can help to squeeze the dispersed phase during droplet breakup which can produce smaller droplets than without the presence of the electric field. Link et al. have reported that the droplet size was reduced remarkably when the applied electric field exceeded the threshold value⁶. Kim et al. also explored the dependence of droplet

sizes on the flow rates and electric field through experiments, and they reported that water-in-oil droplets less than 1 μm were produced in HFFD with the aid of electric field⁷.

Despite these pioneer explorations through experiments, the fundamentals of droplet breakup controlled by electric fields have not been fully understood yet. Many parameters play roles in breakup process, i.e., flow rates of the two phases, fluid viscosity, surface tension, etc., thus make the process complicated to study. As computational fluidic dynamics (CFD) can provide insight of the breakup dynamics, in this paper we presented our numerical simulations to investigate the breakup of silicone oil droplet in water solution. The interface between the immiscible fluids is tracked by conservative level-set method (LSM). Coupled with electric static equation, an additional electric force is added to the Navier-Stokes equation besides the surface tension force. Nie et al. has carried out experimental work of silicon oil-in-water droplet formation process without electric field in 2008⁵. In our previous work, we have studied the breakup dynamics of silicone oil droplets in water without the presence of electric field and obtained good agreements with Nie's observations⁸. Here we add an external static electric field in our model and analyze its effect on droplet breakup. This work may benefit the understanding of droplet formation process under electric fields and provide help to the design and manipulation of droplet-based microfluidics.

2. Use of COMSOL Multiphysics

The electric field is governed by Poisson's equation:

$$\nabla \cdot (\varepsilon \nabla V) = \rho_f \quad (1)$$

where ε is the permittivity of the medium ($\text{C}/(\text{V} \cdot \text{m})$), V is the electric potential (V) and ρ_f is the volumetric free charge density (C/m^3). The electric field \vec{E} (V/m) is related to the electric potential through the equation:

$$\vec{E} = -\nabla V \quad (2)$$

As ε varies across the moving interface, the resulted electric field inside the dispersed phase would change not only strength but also direction. As Maxwell stress plays a key role in the droplet formation process, a suitable model to account for the free charge density ρ_f is

critical. Since electric-neutral fluids are used, the free charge densities in bulk phases are zero. The free charges only present on the interface region. Due to the low conductivities of the two phases (5.5 $\mu\text{S}/\text{m}$ and 10^{-7} $\mu\text{S}/\text{m}$ for water solution and silicone oil respectively), the perfect dielectric model¹⁴ that assumes that no conduction of electric charge exists is used to simply to model. Therefore, ρ_f is 0 for the entire domain, and the Poisson equation is reduced to Laplace equation: $\nabla \cdot (\varepsilon \nabla V) = 0$. The electric field is developed both inside and outside the two-fluid interface, and only polarization charges exist.

The interface is tracked by level-set method (LSM), which tracks the interface by level-set equation ϕ . LSM solves only one-set of Navier-Stokes equations:

$$\frac{\partial \rho}{\partial t} + \nabla \cdot (\rho \vec{u}) = 0 \quad (3)$$

$$\frac{\partial (\rho \vec{u})}{\partial t} + \nabla \cdot (\rho \vec{u} \vec{u}) = -\nabla P + \nabla \cdot [\mu (\nabla \vec{u} + \nabla \vec{u}^T)] + \vec{F}_{sf} + \vec{F}_{ef} \quad (4)$$

where ρ and μ are averaged density and viscosity across the interface, \vec{F}_{sf} is the surface tension force formulated in Eq.(6) and \vec{F}_{ef} is the volumetric electric force. In this study, since the density difference between the two phases is small, gravitational force is neglected.

The properties, such as density ρ , viscosity μ and permittivity ε are smoothed by ϕ across the interface:

$$\rho = \rho_1 + (\rho_2 - \rho_1)\phi$$

$$\mu = \mu_1 + (\mu_2 - \mu_1)\phi$$

$$\varepsilon = \varepsilon_1 + (\varepsilon_2 - \varepsilon_1)\phi$$

where the subscript 1 and 2 denote for the two phases.

The volumetric electric force \vec{F}_{ef} can be calculated by taking the divergence of Maxwell stress tensor (T_{MW}) with the assumption of incompressible fluid

$$\vec{F}_{ef} = \nabla \cdot T_{MW} = -\frac{1}{2}(\vec{E} \cdot \vec{E})\nabla \varepsilon + \rho_f \vec{E} \quad (5)$$

The first term on Eq. (5) is contributed by the polarization stress due to the varying electric permittivity, and it acts on the normal direction across the interface as a result of the term $\nabla \varepsilon$. The second term is zero with the assumption of perfect dielectric. The detail information of the level-set model is referred to our previous work⁸.

The fluid properties used in the simulations are listed in Table 1. The interfacial tension between the two phases is 4.8 mN/m. The variations of fluid properties, i.e., density and interfacial tension between the two types of silicone oil are neglected. Although the electric field can affect the wettability of the fluids, the variation of the contact angle is also neglected.

Table 1 Fluid properties

Liquids	Water	Silicone oil
Density (kg/m^3)	1000	960
Viscosity (cp)	1	50/100
Relative permittivity	78.5	2.8

The geometry of the MFFD and its dimensions are shown in Figure 1. The continuous phase is injected from the two side channels with a constant flow rate Q_c . The dispersed phase, silicone oil, is injected from the center channel with a constant flow rate Q_d . The simulations are performed inside a two-dimensional domain consisting of 13,160 structured elements.

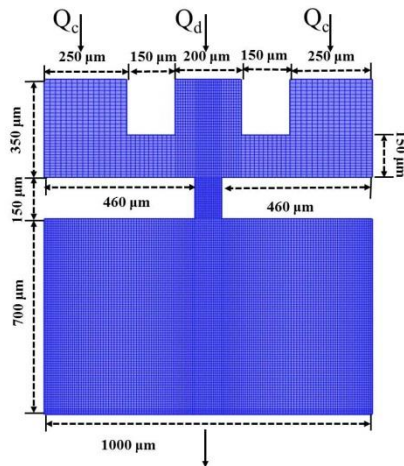


Figure 1 Geometry dimensions of the MFFD and the mesh used for this study. The dimensions of the orifice are: $w_{or} = 80 \mu\text{m}$ and $L = 150 \mu\text{m}$, and it is placed at a distance of $150 \mu\text{m}$ to the upstream channels. The microfluidic channels have a uniform depth as $86 \mu\text{m}$.

All the simulations are performed in Comsol Multiphysics 4.3a. The conservative level-set model is built in Two-phase flow, Level-set Interface in Fluid Flow Module. The Poisson equation is set up in Electrostatic Interface in AC/DC Module. The total simulation time is

selected to ensure at least three droplets can be separated from the dispersed phase. The simulations are performed with 8 processors on Philip high performance computer of Louisiana State University. Typically one case study takes about 24 hours.

3. Results and Discussion

3.1 Overview of controlled droplet breakup by electric field

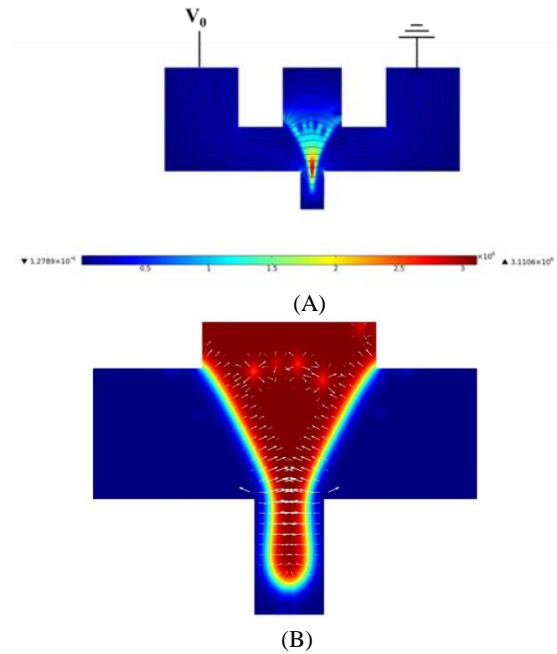


Figure 2 (a) Contour plot of the electric field strength during the droplet formation at $\mu_d=50 \text{ cp}$, $Q_i=25 \text{ mL/h}$ and $Q_o/Q_i=50$. The black lines indicate the electric field lines. A high potential $V_0=240 \text{ V}$ is applied on the left inlet channel of the continuous phase while the right channel is connected to the ground. The color map indicates the magnitude of the electric field strength. (b) Phase surface plot of the focusing region of (a). The white arrows indicate the vectors of the induced electric force by the electric field.

In order to study the effect of electric field on droplet breakup, the left inlet of the continuous phase is connected to a high voltage supply while the right inlet is connected to ground, which creates electric field shown in Figure 2(a). When the silicone oil propagates to the focusing region, the electric field induces polarization charges along the interface. Since the permittivity of the dispersed phase is lower than the continuous phase, positive charges are

accumulated on the left side while negative charges on the right side. As shown in Figure 2(a), during the squeezing stage, the electric field inside the dispersed phase is much higher than in the continuous phase. Shown as the white arrows in Figure 2(b), electric force induced along the interface has two effects: the component on x direction can help to squeeze the dispersed phase during the droplet formation process, and the component on y direction retards the movement of the dispersed phase on y direction.

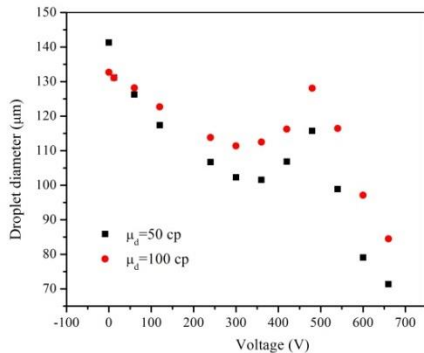


Figure 3 Droplet size as a function of applied voltage.

When different voltages are applied on the left inlet, the obtained droplet sizes are plotted in Figure 3. The droplet size decreases with the applied voltages. Interestingly, there are three zones in the explored voltage ranges. When the voltage is less than 300 V, droplet size decreases almost linearly with applied voltages. This relationship has also been observed by Link⁶ and Kim⁷ respectively in their experiments of which water-in-oil droplets were produced. When voltage of medium strength is applied, the droplet size increases slightly with the applied voltages. As the applied charge exceeds 480 V, the droplet size decreases with the applied voltages again. Obviously, the dynamics of the droplet formation are different in these regions. In the following parts, these dynamics are discussed in detail.

3.2 Droplet breakup with low applied voltages

As shown in Figure 3, if low voltage is applied (0~240 V), the droplet size decreases with the applied voltages. The droplet formation processes with applied voltages of 60 V and 240 V are shown in Figure 4. The corresponding

upstream pressure evolutions are shown in Figure 5.

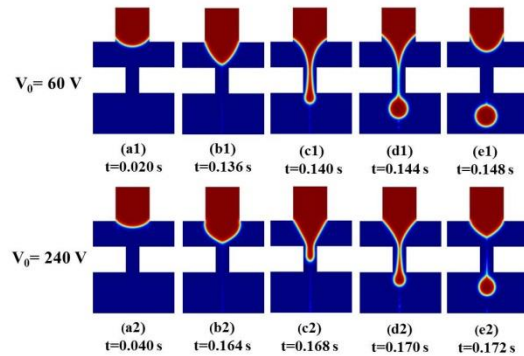
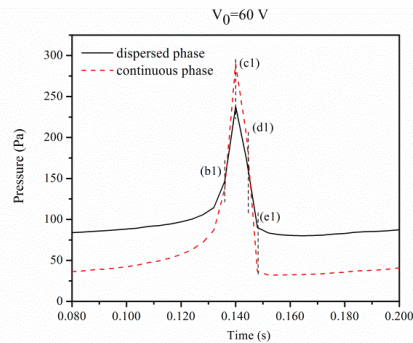
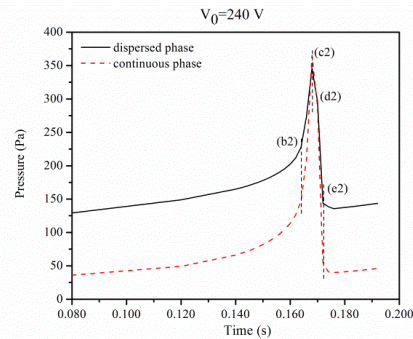


Figure 4 Droplet formation process with low applied voltages at $\mu_d=50$ cp, $Q_i=25$ mL/h and $Q_o/Q_i=50$. (a1)~(e1): 60 V is applied (a2)~(e2): 240 V is applied.



(a)



(b)

Figure 5 Upstream pressure evolutions of the two phases for the droplet breakup process at $\mu_d=50$ cp, $Q_i=25$ mL/h and $Q_o/Q_i=50$. (a) 60 V is applied (b) 240 V is applied. The (b1)~(e1) and (b2)~(e2) correspond to the stages shown in Figure 4. The black dash line indicates the location of corresponding stages shown on the curves.

When the dispersed phase propagates orifice, the upstream pressure increases thus to penetrate the continuous phase. Since it blocks the flow

path, the pressure in continuous phase also increases (stage (b1)). When the interface enters the orifice, the confinement elevates the pressure of both phases, especially of the continuous phase due to its large flow rate (stage (c1)). As the continuous phase has higher pressure, it squeezes the dispersed phase, and a visible neck is formed inside the orifice (stage (d1)). The effects of viscous stress, the pressure difference and the electric stress simultaneously exert on the neck until it is squeezed to a critical value. The surface tension force quickly snaps neck, thus a droplet of defined shape is formed (stage (e1)).

If compare the droplet formation process at 60 V and 90 V, one can notice several differences. One is that the droplet size is reduced with increase of voltage. The strengthened electric force squeezes the neck faster thus reduces the droplet formation time. Another difference is that the dispersed phase spends more time to reach the orifice entrance for 90 V case than the 60 V case (stage (a) to (b)). This is caused by the increased retardation effect exerted by the electric force. To overcome the electric force in y direction, the dispersed phase has to build up higher pressure so as to maintain the flow. Meanwhile, the pressure in the continuous phase does not increase noticeably as shown in Figure 5(b). Therefore, the dispersed phase expands in x direction during its propagation to the orifice.

3.3 Droplet breakup with medium voltages

When the applied voltage is above 240 V, Figure 3 exhibits a transition zone where the droplet size slightly increases with voltage. Figure 6 shows a droplet breakup process in this zone. Compared to those cases of low voltages, the dispersed phase spends longer time to reaches the orifice entrance. Due to the enhanced retardation effect of higher electric fields, its expansion in x direction becomes more noticeable. Also, a much high pressure in the dispersed phase has to be built up to overcome the y component of the electric force. The corresponding pressure evolution indicates that the upstream pressure in the dispersed phase exceeds that of the continuous phase during the entire droplet breakup process. During squeezing (stage (b) to (e)), the dispersed phase tends to expand inside orifice due to its higher pressure

than the continuous phase. Thus, this effect stabilizes the neck and it takes longer time for the x component of the electric force and viscous force to squeeze the neck to critical length, leading to droplet of slightly increased sizes.

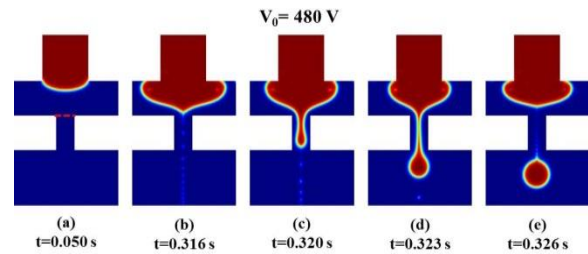


Figure 6 Droplet formation under low electric field at $\mu_d=50$ cp, $Q_i=25$ mL/h and $Q_o/Q_i=50$ with applied voltage of 480 V.

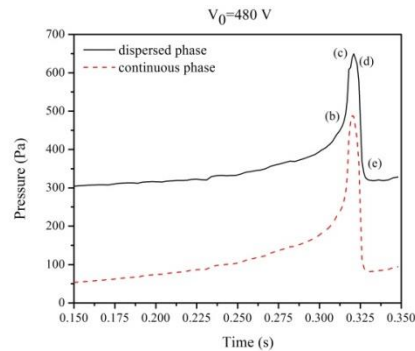


Figure 7 Upstream pressure evolutions at $\mu_d=50$ cp, $Q_i=25$ mL/h and $Q_o/Q_i=50$ with applied voltage of 480 V.

As one can see, the electric force is competing with itself in terms of the control on droplet sizes. Its x component tends to squeeze the neck of the dispersed phase to reduce the droplet formation time. Its y component retards the dispersed phase and make its pressure increase. The increased pressure in turn stabilizes the neck thus elongates the formation time. The latter starts to dominant the droplet breakup from the medium voltage region.

3.4 Droplet breakup with high voltages

Similar to the formation process in medium voltage region, if high voltages are applied, the dispersed phase expands further in x direction as shown in Figure 8. The neck evolutions shown in Figure 9 indicates that the dispersed phase pressure dominants that of the continuous phase.

But the obtained droplet sizes decreases with quickly applied voltages as shown in Figure 3.

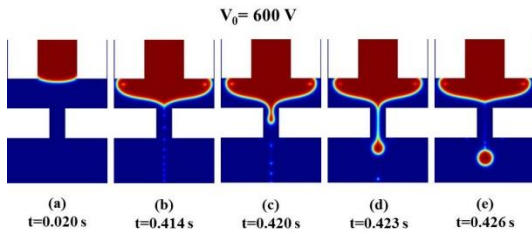


Figure 8 Upstream pressure evolutions at $\mu_d=50$ cp, $Q_i=25$ mL/h and $Q_o/Q_i=50$ with applied voltage of 600 V.

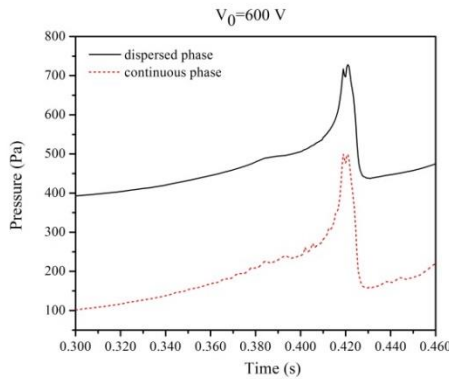


Figure 9 Upstream pressure evolutions at $\mu_d=50$ cp, $Q_i=25$ mL/h and $Q_o/Q_i=50$ with applied voltage of 600 V.

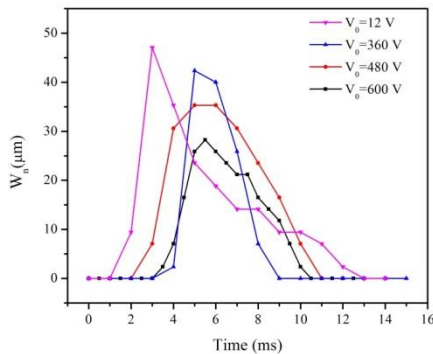


Figure 10 Neck evolutions at various applied voltages in the orifice entrance. The width W_n is measured in the orifice entrance which is marked as red dash line in Figure 6(a).

As shown in Figure 8, the strong electric field leads to a broad deformation of the dispersed phase before it enters the orifice. Although the high pressure in the dispersed phase can stabilize the neck, the maximum width of the neck decreases with applied voltages as shown in Figure 10. Especially when very high

voltage is applied, the maximum neck width is very small that the neck can be quickly squeezed to the critical value. In this region, the droplet size decreases with voltage again.

7. Conclusions

In present work, we have employed level-set method coupled with the perfect dielectric model to study the droplet breakup process under the applied electric field. When the dispersed phase has a much higher viscosity than the continuous phase, solely increasing the flow ratio has shown insignificant effect on reducing the droplet size. But the electric field has shown its unique ability by exerting electric force on the interface. The external electric field has affected the breakup dynamics and form three different regimes. When low electric field is applied, the electric field helps to compress the neck of the dispersed phase, resulting approximately linear decrease in droplet size. When the applied voltage increases to the medium voltage region, the dispersed phase has shown significant expansion due to the retardation effect from the electric force. To overcome the retardation force, a high pressure is developed in the dispersed phase which stabilizes the neck during the breakup process. In this region, the droplet size increases with the applied voltages. Further increase of the applied voltage reduces the width of the neck during the breakup. Because of the small neck width, the neck is quickly squeezed to the critical pinch-off condition. Therefore, the droplet size reduces with voltage again.

5. References

1. A. Gunther, Multiphase microfluidics: from flow characteristics to chemical and material synthesis, *Lab on a Chip*, **6**, 1487-1503 (2006).
2. H. Song, Reactions in droplets in microfluidic channels, *Angew. Chem.-Int. Edit.*, **45**, 7336-7356 (2006)
3. J.D. Tice, Formation of droplets and mixing in multiphase microfluidics at low values of the Reynolds and the Capillary numbers, *Langmuir*, **19**, 9127-9133 (2003)
4. S.L. Anna, Formation of dispersions using “flow focusing” in microchannels, *Applied Physics Letters*, **82**, 364-366 (2003)
5. Z.H. Nie, Emulsification in a microfluidic flow-focusing device: effect of viscosities of the

liquids, *Microfluid. Nanofluid.*, **5**, 585-594 (2008)

6. D.R. Link, Electric control of droplets in microfluidic devices, *Angew. Chem.-Int. Edit.*, **45**, 2556-2560 (2006)

7. H.Kim, Controlled production of emulsion drops using an electric field in a flow-focusing microfluidic device, *Applied Physics Letters*, **91**, (2007)

8. Y. Li, Numerical study of droplet formation inside a microfluidic flow-focusing device, *Proceedings of the 2012 Comsol Conference in Boston* (2012).

6. Acknowledgements

The authors would like to acknowledge the computing facilities of the Louisiana Optical Network Initiative (LONI) & High Performance Computing (HPC) facility at Louisiana State University and the continued funding from the Cain Chair Program.